Absorption and generation of femtosecond laser-pulse excited spin currents in noncollinear magnetic bilayers

PHYSICAL REVIEW B **96**, 014417 (2017)

Absorption and generation of femtosecond laser-pulse excited spin currents in noncollinear magnetic bilayers

M. L. M. Lalieu,* P. L. J. Helgers, and B. Koopmans
Department of Applied Physics, Institute for Photonic Integration, Eindhoven University of Technology, P.O. Box 513, 5600 MB Eindhoven, The Netherlands
(Received 21 April 2017; published 13 July 2017)

Spin currents can be generated on an ultrafast time scale by excitation of a ferromagnetic (FM) thin film with a femtosecond laser pulse. Recently, it has been demonstrated that these ultrafast spin currents can transport angular momentum to neighboring FM layers, being able to change both the magnitude and orientation of the magnetization in the adjacent layer. In this paper, both the generation and absorption of these optically excited spin currents are investigated. This is done using noncollinear magnetic bilayers, i.e., two FM layers separated by a conductive spacer. Spin currents are generated in a Co/Ni multilayer with out-of-plane (OOP) anisotropy, and absorbed by a Co layer with an in-plane (IP) anisotropy. This behavior is confirmed by careful analysis of the laser-pulse induced magnetization dynamics, whereafter it is demonstrated that the transverse spin current is absorbed very locally near the injection interface of the IP layer (90% within the first ≈2 nm). Moreover, it will also be shown that this local absorption results in the excitation of THz standing spin waves within the IP layer. The dispersion measured for these high-frequency spin waves shows a discrepancy with respect to the theoretical predictions, for which an explanation involving intermixed interface regions is proposed. Lastly, the spin current generation is investigated by using magnetic bilayers with a different number of repeats for the Co/Ni multilayer, which proves to be of great relevance for identifying the optical spin current generation mechanism.

DOI: 10.1103/PhysRevB.96.014417

I. INTRODUCTION

The discovery of ultrafast demagnetization in ferromagnetic (FM) thin films after femtosecond (fs) laser-pulse excitation induced a growing interest in the field of fs magnetization dynamics. Two decades ago, Beaurepaire *et al.* demonstrated that the magnetization in a Ni thin film can be quenched to almost half its initial value within a picosecond after the excitation [1]. Although the discovery triggered an interesting debate on the physical mechanism responsible for the rapid loss of magnetization [2–6], its relevance for fast and energy efficient magnetic data storage was quickly recognized. This realization eventually led to the discovery of all-optical magnetization reversal in both (synthetic) ferrimagnets [7,8] and ferromagnets [9].

A third important discovery was that spin currents are generated upon excitation of a FM film. This was first demonstrated in a collinear magnetic bilayer, where angular momentum transfer through the spacer layer resulted in a faster and larger demagnetization of the two antiparallel FM layers [10]. Several more recent studies have confirmed these laser-pulse induced spin currents [11–16]. It has even been claimed that the optically excited spin current can enhance the magnetization in one of the FM layers of the magnetic bilayer [12]. Nowadays, *electrically* generated spin currents are heavily used in the field of spintronics, where they are exploited to control the direction of the magnetization in a FM layer via the spin transfer torque (STT). A similar control of the magnetization on an ultrafast time scale can be established using an *optically* generated spin current, as was recently demonstrated using a noncollinear magnetic bilayer [14–16]. It was argued that this optical-STT is an accurate probe of the spin current, and it will be employed in this work to investigate both the generation and absorption of the laser-pulse induced spin current.

Since its discovery, several mechanisms for the generation of an optical spin current have been suggested. Battiato *et al.* proposed a mechanism based on the spin-dependent transport of excited electrons. In this model, a superdiffusive spin current is generated due to spin filtering of the hot electrons in the FM layer [5]. A second mechanism uses the spin-dependent Seebeck effect to explain the optical generation of spin currents [16]. In this case, the spin current is generated due to a temperature gradient across the FM material caused by the laser excitation. Lastly, there are models in which the spin current is generated by demagnetization, for instance, using magnon-electron coupling. In this case, electrons become spin polarized due to the excitation of magnons and the conservation of angular momentum, acting as a source for a diffuse spin current that follows dM/dt [15].

In this paper, the generation of the fs laser-pulse excited spin current is investigated in order to identify which mechanism is at play. Besides the spin current generation, also the absorption depth of the spin current in a second FM layer is investigated. Both phenomena are studied using a noncollinear magnetic bilayer. This magnetic bilayer consists of one FM layer with an out-of-plane (OOP) anisotropy (generation layer), and a second FM layer with in-plane (IP) anisotropy (absorption layer). The two FM layers are separated by a metallic (nonmagnetic) spacer layer. By varying the thickness of the generation layer the thickness dependence of the spin current generation is examined. It is found that the generation of spin currents is almost independent on the thickness of the generation layer. Using a wedged absorption layer, the absorption of the spin current is investigated, revealing an

*m.l.m.lalieu@tue.nl

absorption depth in Co of 2–3 nm. It will be demonstrated that this very local absorption near the interface allows for THz spin wave excitation in these noncollinear magnetic bilayers, as was recently also demonstrated by Razdolski *et al.* [17], and being of great relevance for the upcoming field of (THz) magnonics [18,19].

II. SAMPLE STRUCTURE AND CHARACTERIZATION

The basic structure of the noncollinear magnetic bilayers used in this paper is SiB(substrate)/Ta(2)/Pt(4)/$[\mathrm{Co}(0.2)/\mathrm{Ni}(0.6)]_N$/Co(0.2)/Cu(5)/Co($t_{\mathrm{Co}}$)/Pt(1) (thickness in nm). All samples are fabricated using dc magnetron sputtering at room temperature. In this structure, the Co/Ni multilayer has an easy axis along the OOP direction [perpendicular magnetic anisotropy (PMA)], and the top Co layer has an easy plane along the in-plane direction. The two FM layers are separated by a 5-nm-thick Cu layer which allows for the transfer of spin currents and decouples both FM layers. The measurements are performed using a standard time-resolved magneto-optic Kerr effect setup (TR-MOKE) in the polar configuration, and in the presence of an external field that is applied parallel to the sample surface. The probe and pump pulses have a spot size of $\approx$10 μm and a pulse length of $\approx$150 fs. The pulses are produced by a Ti:sapphire laser with a wavelength of 790 nm and a repetition rate of 80 MHz. In the experiments, the pump pulse is used to excite the spin dynamics, and the probe pulse is used to measure the time-resolved OOP magnetization component of both FM layers of the noncollinear bilayer.

The dynamics in the noncollinear system during the measurements is illustrated by the cartoon in Fig. 1(a). Before excitation, the system is in a *steady state*, where the in-plane field sets the direction of the IP magnetization as well as a slight canting of the OOP magnetization (depending on its PMA). When the structure is *excited* by the laser pulse, spin currents are generated in both layers. These spin currents will flow through the spacer layer to be injected in the other layer. The transverse spins injected in each layer will be *absorbed*, resulting in a spin transfer torque (STT) on the magnetization. As a result, the magnetization is canted away from the effective field, and a damped *precession* is initiated. Using the probe pulse, the precessions can be measured by measuring the OOP magnetization as a function of time. The amount of initial canting of the magnetization in each layer, i.e., the initial amplitude of the damped precession, is proportional to the absorbed angular momentum. In this paper, the precession amplitude of the IP layer, in combination with the demagnetization of the OOP layer, is used to investigate the absorption and generation of the spin current generated in the OOP layer. The precession in the OOP layer is not visible in the measurements due to the smaller MO sensitivity to the (bottom) OOP layer compared to the (top) IP layer, as will be shown in the following.

A typical measurement performed on a noncollinear bilayer with $N = 4$ and $t_{\mathrm{Co}} = 3$ nm is shown in Fig. 1(a). In this figure the OOP magnetization of both layers, normalized to the magnetization of the OOP layer, is plotted as a function of the pump-probe delay. In the first few picoseconds the demagnetization and subsequent remagnetization of the OOP layer is visible. On the long time scale a clear precession of $\approx$10 GHz is observed. As is illustrated in the cartoon of Fig. 1(a), the optical generated spin currents are expected to induce a precessional motion of both the IP and OOP magnetization. Moreover, a precession in both FM layers was measured in previous experiments by Schellekens *et al.* [14], using similar structures. In their work, it was demonstrated that the precession of the IP magnetization was indeed initiated by the *STT mechanism* discussed earlier. The precession of the OOP magnetization, however, was attributed to a laser-pulse induced anisotropy change, which was called the ΔK *mechanism* and will be discussed in more detail later. In this paper, the precession in the IP layer will be used to measure the absorption and generation of the spin current generated in the OOP layer. Therefore, it needs to be confirmed that the measured precession actually is the precessional motion of the IP magnetization, initiated by the STT mechanism. In the following, it will be shown that this is indeed the case.

One way to identify to which layer the precession corresponds is to perform field-dependent precession measurements. In case of the IP magnetization in an in-plane external field, the frequency f_{IP} is given by the Kittel relation

$$f_{\mathrm{IP}} = \frac{\gamma}{2\pi}\sqrt{B_{\mathrm{app}}\left(B_{\mathrm{app}} + \mu_0 M_{\mathrm{s}} - \frac{2K_{\mathrm{s}}}{tM_{\mathrm{s}}}\right)}, \tag{1}$$

in which γ is the gyromagnetic ratio, B_{app} is the applied field, t and M_{s} the thickness and saturation magnetization of the magnetic layer, and K_{s} the surface anisotropy constant (including the contribution of both interfaces of the FM layer). In the case of the OOP magnetization in an in-plane field, where the applied field is small compared to the anisotropy field, the precession frequency f_{OOP} is given by

$$f_{\mathrm{OOP}} = \frac{\gamma}{2\pi}\sqrt{\left(\mu_0 M_{\mathrm{s}} - \frac{2K_{\mathrm{s}}}{tM_{\mathrm{s}}}\right)^2 - B_{\mathrm{app}}^2}. \tag{2}$$

From these equations it is seen that in the case of the IP (OOP) magnetization, the frequency increases (decreases) when the applied field is increased. Figure 1(b) shows the measured frequency as a function of the applied field (black dots). A clear increase of the frequency with field is observed. Moreover, the field dependence is nicely fitted with the Kittel relation of Eq. (1) (red curve), resulting in a saturation magnetization of 1.3–1.4 MA m^{-1}, using a surface anisotropy of 0.3–0.6 mJ m^{-2} derived from the literature [20] and $\gamma = 1.76 \times 10^{11}$ rad s^{-1} T^{-1}. The found saturation magnetization compares well with the bulk value for Co of 1.4 MA m^{-1}, unambiguously demonstrating that it is the precessional motion of the IP magnetization that is measured.

Next, it should be verified that the mechanism initiating the precession is indeed the STT mechanism, and not the earlier mentioned ΔK mechanism or a magnetostatic coupling due to orange-peel coupling. An analysis on the magnetostatic coupling for similar structures has already been performed by Schellekens *et al.*, ruling out orange-peel coupling to be the source of the observed precessions [14]. The ΔK mechanism arises when the field is applied at a certain angle to the sample surface [21], i.e., due to a minor misalignment. With the field at an angle, the equilibrium direction of the effective

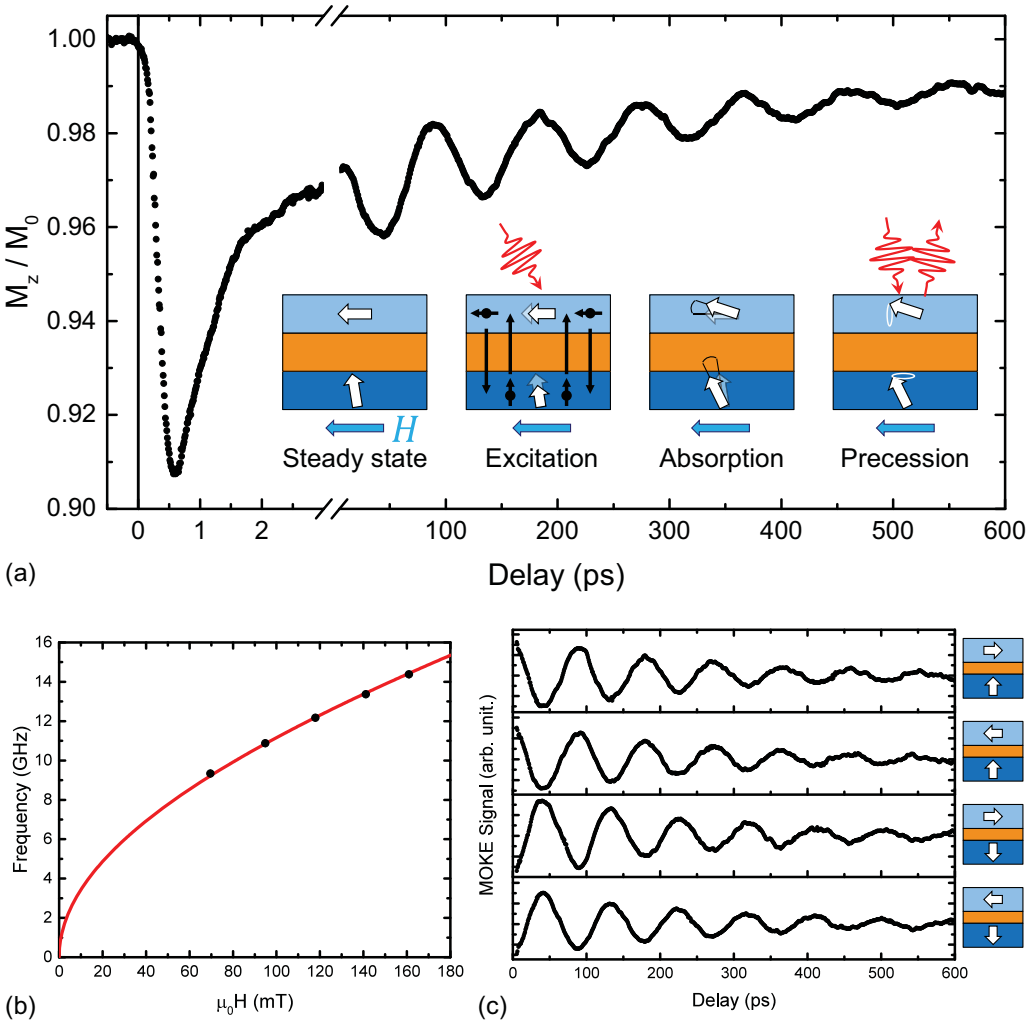

FIG. 1. The measurements performed on a noncollinear system with $N = 4$ and $t_{Co} = 3$ nm. (a) Typical precession measurement with an in-plane applied field of 95 mT. The demagnetization of the OOP layer is visible in the first picosecond, and a clear precession (≈10 GHz) is present on the long time scale. The cartoon shows the different stages before, during and after the optical excitation. (b) Precession frequency measured as a function of the in-plane applied field. The solid line represents the fit using the Kittel relation, resulting in a saturation magnetization of 1.3−1.4 MA m^{-1}, using a surface anisotropy of 0.3−0.6 mJ m^{-2} taken from literature [20] and $\gamma = 1.76 \times 10^{11}$ rad s^{-1} T^{-1}. (c) Precession measurements for all combinations of IP field direction (parallel to IP magnetization) and OOP magnetization direction (remagnetization of OOP layer subtracted from the signal).

field and thus the magnetization is no longer IP, but is canted slightly out of plane. A precession can be initiated by a laser-pulse induced change in the magnetization and anisotropy, abruptly altering the effective field direction and resulting in a precession of the magnetization. Fortunately, a distinction between the two mechanisms can be made by looking at the sign of the measured precession when the applied field and OOP magnetization directions are inverted. In the case of the ΔK mechanism, the precession signal inverts with the field direction, but is independent of the OOP magnetization direction. On the contrary, for the STT mechanism, the precession signal is independent of the field direction, and is inverted when the magnetization direction of the OOP layer reverses. Figure 1(c) shows the precession measured for all combinations of IP field direction (parallel to IP magnetization) and OOP magnetization direction. Looking at the top two curves, it can be seen that the precession is identical for both field directions. The precession signal inverts when the OOP magnetization direction is reversed, as can be seen in the bottom two curves. This confirms that the measured precession of the IP magnetization is indeed initiated by the STT mechanism.

It was noted before that in previous experiments on similar structures performed by Schellekens *et al.*, also a precession of the OOP magnetization was measured, which was initiated by the ΔK mechanism [14]. The absence of this precession in the present measurements is caused by the addition of a Ta seed layer underneath the Co/Ni multilayer, causing a strong increase in the PMA and the corresponding anisotropy field. With an increase of the anisotropy field of the OOP layer, the effect of the laser-pulse excitation on the effective field becomes smaller, reducing the amplitude of the ΔK precession to a point where it is no longer measurable. The exclusion of the precession of the OOP magnetization from

the measurements allows for a more straightforward analysis of the measured data.

With the measured spin dynamics verified, it can be used to investigate the generation and absorption of the laser-pulse excited spin current. To do so, two parameters are defined, the *efficiency* ϵ and the *initial canting angle* θ_c. The efficiency is defined as the ratio of OOP angular momentum absorbed per unit area by the IP layer, $\Delta\mathcal{M}_{z,\mathrm{IP}}$, to the angular momentum lost per unit area during demagnetization by the OOP layer, $\Delta\mathcal{M}_{z,\mathrm{OOP}}$,

$$\epsilon = \frac{\Delta\mathcal{M}_{z,\mathrm{IP}}}{\Delta\mathcal{M}_{z,\mathrm{OOP}}}. \tag{3}$$

The initial canting angle is defined as the angle of the IP magnetization with respect to the sample surface after absorption of the OOP spin current, and can be calculated using

$$\theta_c = \arcsin\left(\frac{\Delta\mathcal{M}_{z,\mathrm{IP}}}{M_{s,\mathrm{IP}}t_{\mathrm{IP}}}\right). \tag{4}$$

In this equation, $M_{s,\mathrm{IP}}$ and t_{IP} are the saturation magnetization and thickness of the IP layer, respectively. A discussion on how the efficiency and canting angle are derived from a precession measurement as shown in Fig. 1(a) can be found in Supplemental Material Sec. I [22].

It is important to note that measurements on different samples or different areas on the same sample are going to be compared. The amount of demagnetization in these different measurements might be slightly different, e.g., due to a small difference in spot size or pump-probe overlap. In order to be able to compare the different measurements, care should be taken that the measured parameters are independent of the demagnetization of the OOP layer. This is investigated by measuring θ_c as a function of the demagnetization of the OOP layer for a noncollinear system with $N = 4$ and $t_{\mathrm{Co}} = 3$ nm. The results of this measurement are presented by the black dots in Fig. 2. The figure shows that for the low demagnetization regime used throughout this paper, θ_c is linear in the amount of demagnetization (red line). The achieved θ_c is on the order of millidegrees, and thus can be approximated by $\Delta\mathcal{M}_{z,\mathrm{IP}}/(M_{s,\mathrm{IP}}t_{\mathrm{IP}})$. This means that $\Delta\mathcal{M}_{z,\mathrm{IP}}$ scales linearly with the demagnetization, i.e., with $\Delta\mathcal{M}_{z,\mathrm{OOP}}$, and thus that the efficiency is independent of the amount of demagnetization. Moreover, the linear dependence of θ_c shown in Fig. 2 also means that the canting angle per percent demagnetization $\theta_{c,\%}$ can be used as a demagnetization-independent parameter. In conclusion, both ϵ and $\theta_{c,\%}$ are good parameters to be compared between different measurements.

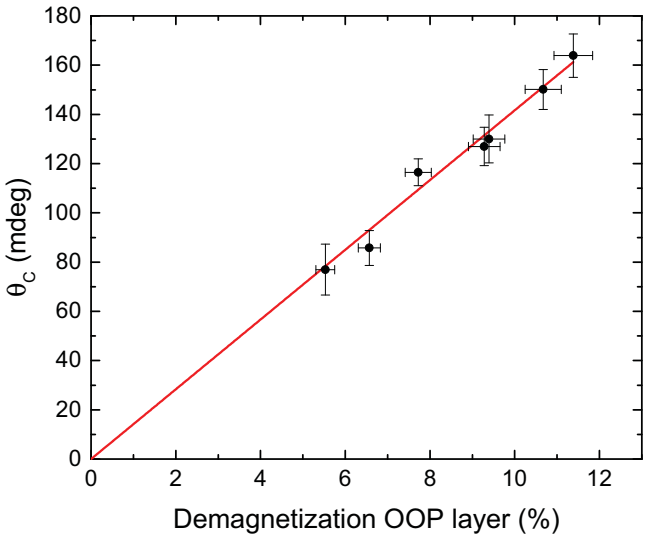

FIG. 2. Fluence dependent measurement performed on a noncollinear system with $N = 4$ and $t_{\mathrm{Co}} = 3$ nm. The figure shows the measured canting angle of the IP magnetization as a function of the demagnetization of the OOP layer. The solid line represents a linear fit with fixed zero offset.

III. RESULTS AND DISCUSSION

A. Spin current absorption and THz spin wave excitation

First, the absorption of the spin current in the IP layer is investigated. By using a wedge-shaped top Co layer, the penetration depth of the transverse spins is measured. The structure used in this measurement is given by the basic noncollinear bilayer introduced earlier, now with $N = 4$ and a wedge-shaped top Co layer with t_{Co} ranging from 0 to 6 nm over a distance of 20 mm. Using the fact that the TR-MOKE measurement is a very local technique (spot size $\approx$10 μm), the thickness-dependent measurement can be performed by measuring ϵ and $\theta_{c,\%}$ at different points along the Co wedge.

The saturation magnetization and surface anisotropy of the wedged IP layer, needed for the determination of ϵ and $\theta_{c,\%}$, are obtained by measuring the frequency of the precession as a function of the IP layer thickness. The Kittel relation [Eq. (1)] shows that indeed the thickness dependence of the anisotropy term allows one to determine both $M_{s,\mathrm{IP}}$ and K_s from the measured data. The measured frequencies as a function of the Co layer thickness, for different applied field strengths, are shown by the solid dots in Fig. 3(a). The solid curves are fits to the data using Eq. (1). The fits are performed using a global fit with shared fitting parameters $M_{s,\mathrm{IP}}$ and K_s, resulting in $M_{s,\mathrm{IP}} \approx 1240$ kA m^{-1} and $K_s \approx 0.70$ mJ m^{-2}. Looking at the fitted curves, it can be seen that the measured data are not well described by the Kittel relation. For all field strengths it seems that there is an additional thickness dependence that is not captured by Eq. (1). As will be discussed later, one possibility is a thickness-dependent saturation magnetization, decreasing for thinner layer thicknesses. For simplicity, however, the simplest case with constant $M_{s,\mathrm{IP}}$ and K_s throughout the wedged layer will be used in the remainder of this discussion. The analysis including a thickness-dependent $M_{s,\mathrm{IP}}$ can be found in Supplemental Material Sec. III [22] [results are shown by the dashed curves in Fig. 3(a)]. There it is shown that the overall behavior of the efficiency and canting angle as a function of the Co layer thickness is robust and similar for both cases.

The efficiency calculated as a function of the top Co layer thickness is shown in Fig. 3(b) (solid dots). For the very thin Co thicknesses (gray area) no precession amplitudes could be determined, which is attributed to the surface anisotropy (PMA) becoming too pronounced. The solid curve is a fit to

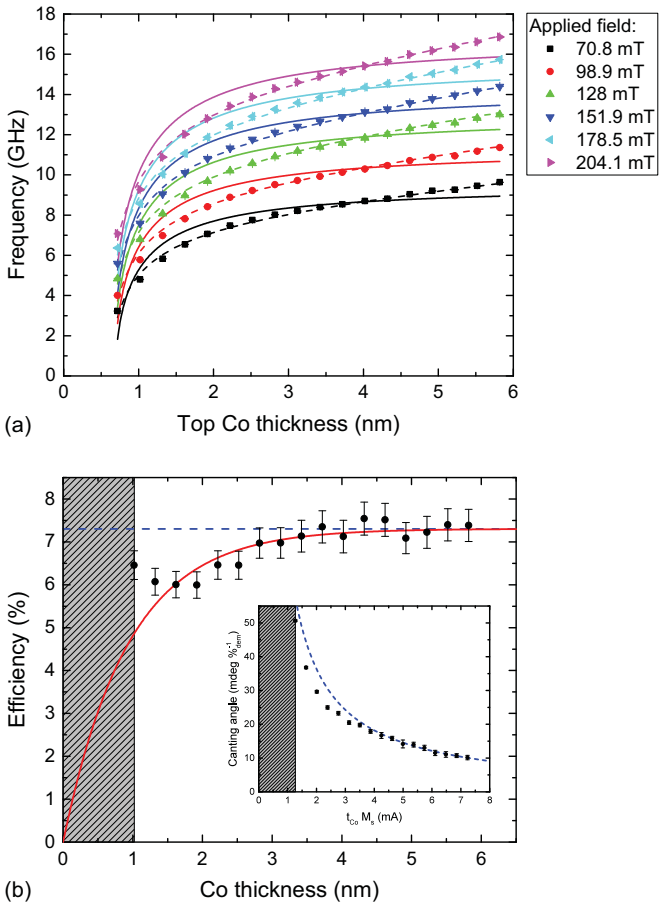

FIG. 3. Measurements performed on a noncollinear magnetic bilayer with $N = 4$ and wedged top Co layer with thickness ranging from 0 to 6 nm over a distance of 20 mm. (a) Precession frequency measured as a function of top Co layer thickness for six different in-plane applied field strengths. The solid curves represent fits using the standard Kittel relation, resulting in $M_{s,IP} \approx 1240\,\mathrm{kA\,m^{-1}}$ and $K_s \approx 0.70\,\mathrm{mJ\,m^{-2}}$. The dotted curves represent fits using the Kittel relation including a thickness dependent saturation magnetization. (b) Efficiency and canting angle per percent demagnetization (inset) as a function of top Co layer thickness. The solid curve represents a fit to the data showing a finite absorption depth (i.e., 90% absorbed within first 2.1 ± 0.2 nm). The dotted lines represent constant efficiency and corresponding $\theta_{c,\%}$, which describes the case when there is full absorption independent of top Co layer thickness.

the data following

$$\epsilon = \epsilon_{max}\left(1 - e^{-\frac{t_{Co}}{\lambda_{t,Co}}}\right), \tag{5}$$

where ϵ_{max} is the efficiency for infinite Co thickness t_{Co}, and λ_{Co} the characteristic spin absorbtion length. For the thinnest Co thicknesses, the efficiency shows a small increase, deviating from the behavior of Eq. (5). This deviation is mainly the result of using the simplest case with constant $M_{s,IP}$ and K_s. The deviation is less pronounced when a thickness-dependent $M_{s,IP}$ is used in the analysis, of which the result is shown in Supplemental Material Sec. III [22]. For large thicknesses, the efficiency saturates, corresponding to full absorption of the transverse spin current. At zero thickness, i.e., no IP layer, the efficiency must be zero. Looking back at the definition of the efficiency [Eq. (3)], it can be seen that the behavior shown in Fig. 3(b) corresponds to a transverse spin absorption that decays exponentially with the distance from the interface where the spins are injected. From the fit, the values $\lambda_{Co} = 0.93 \pm 0.07$ nm and $\epsilon_{max} = 7.3 \pm 0.1\%$ are obtained. This result shows that the spin current is absorbed very locally near the interface, i.e., 90% of the transverse spins are absorbed within the first 2.1 ± 0.2 nm of the Co layer. This penetration depth agrees well with the penetration depth of 1.7 nm found for electrically driven transverse spin currents in Co by Ref. [23].

The effect of the limited penetration depth of the transverse spins is also seen in the canting angle per percent demagnetization, as shown in the inset of Fig. 3(b). Here, $\theta_{c,\%}$ is plotted as a function of $t_{Co}M_s$ (solid dots). For small canting angles, a $(t_{Co}M_s)^{-1}$ dependency is expected when there is full absorption, i.e., constant efficiency ($\lambda_{Co} \to 0$ nm), illustrated by the dotted curve. It is seen that for Co thicknesses below approximately 3 nm the canting angle is not reaching its maximum value, demonstrating again the incomplete absorption of the spin current for these thicknesses.

The results on the spin absorption show that the absorption of the transverse spins falls off exponentially with the distance from the injection interface. This results in a strong gradient in the canting angle of the IP magnetization, as illustrated in the left cartoon of Fig. 4(a). It was recently demonstrated by Razdolski *et al.* that a strong gradient in the magnetization direction can be used to excite THz standing spin waves along the depth of the IP layer [17]. In the following, it will be demonstrated that these THz spin waves, with frequencies up to 1.2 THz, are indeed excited in the noncollinear bilayer measured here.

The THz spin waves are observed as an additional precession on the fast picosecond time scale in the demagnetization measurements performed in the thicker region of the Co wedge (not shown). The spin waves carry no net OOP magnetic moment, causing their signal to be averaged out in the case of homogeneous averaging across the thickness of the layer. The fact that the spin waves can be measured in the TR-MOKE setup results from a certain depth sensitivity due to the attenuation of the laser within the FM layer. However, for these thin layers, the depth sensitivity and thereby the spin wave signal are only small. To achieve a better sensitivity of the TR-MOKE setup to the THz precession, a quarter-wave plate (QWP) was added to the probe beam. By carefully tuning the QWP angle, a specific linear combination of Kerr rotation and ellipticity can be measured [24], and the signal can be optimized to measure the THz precession. An example of such a measurement is shown in Fig. 4(a). In this figure, both the first-order standing spin wave (0.55 THz) as well as the fundamental precession (10 GHz) are visible (different time scales), both illustrated in the right cartoon in the figure. The shown measurement is performed with an IP layer thickness of $t_{Co} = 5.5$ nm. The sign of the THz precession has the same dependency on the IP and OOP magnetization direction as the fundamental precession, which was shown in Fig. 1(c). Also, the THz precession is even present without the applied field, which is expected with the exchange interaction driving the precession.

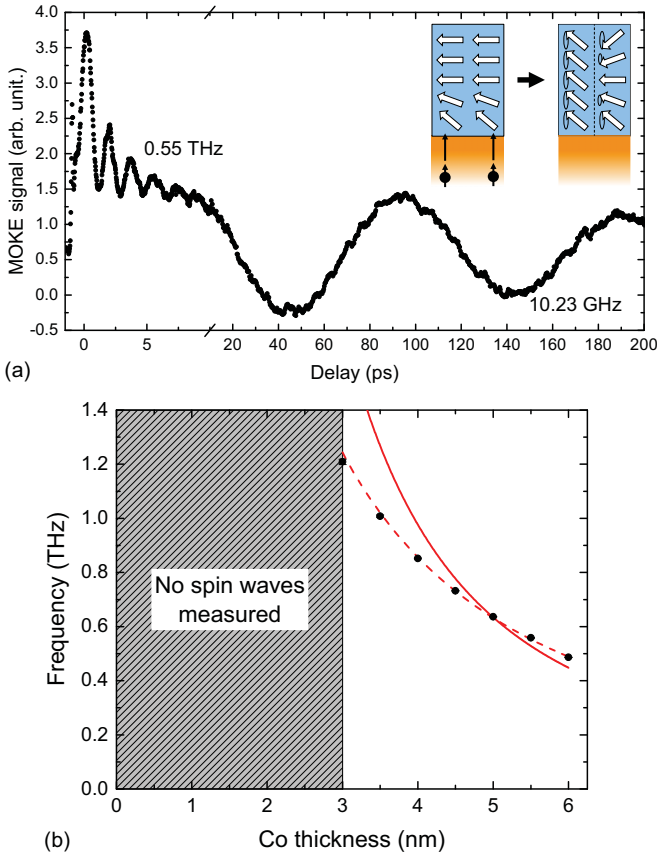

FIG. 4. (a) Precession measurement performed on a noncollinear bilayer with $N = 4$ and wedged top Co layer with a thickness ranging from 0 to 6 nm, measured at a thickness of 5.5 nm. During the measurement a QWP was added to TR-MOKE setup to increase the sensitivity to the THz precession. Both the spin wave (≈0.55 THz) and the fundamental precession (≈10 GHz) are visible. The cartoon shows the gradient in the canting angle within the Co layer after the optical excitation, and the resulting fundamental and first order standing spin wave. (b) Spin wave frequency measured as a function of the Co layer thickness. No THz precessions are found for Co thicknesses below 3 nm. The solid curve represents a fit using the standard dispersion relation, showing a clear discrepancy with the measured data. The dotted curve represents a fit using the dispersion relation with a thickness dependent spin wave stiffness, showing a much more accurate description of the data.

Using the wedge shape of the IP layer in the noncollinear bilayer, the spin wave frequency can be measured as a function of the Co layer thickness. The frequencies measured for the different Co thicknesses are shown by the black dots in Fig. 4(b). At thicknesses of 2.5 nm and below, there was no sign of the spin wave in the measurement. This means that either the spin waves are not excited, or that they are not visible in the measurement. At the moment it is believed that the latter is the case, being the result of a strong decrease in the lifetime of the spin waves due to the large increase in frequency, combined with a decrease in the depth sensitivity of the MOKE for the thinner layers.

The thickness dependence of the spin wave frequency shown in Fig. 4(b) can be fitted using the theoretical dispersion relation. This dispersion relation, including both the in-plane applied field (B_{app}) and shape and surface anisotropy contributions, is given by (see Supplemental Material Sec. II [22] for the derivation)

$$f(k) = \frac{\gamma}{2\pi}\left[\left(B_{app} + \frac{D_{sw}}{\gamma\hbar}k^2\right) \times \left(B_{app} + \mu_0 M_s - \frac{2K_s}{tM_s} + \frac{D_{sw}}{\gamma\hbar}k^2\right)\right]^{1/2}, \quad (6)$$

$$k = \frac{\pi n}{t}. \quad (7)$$

In this equation, the spin wave frequency and order are given by f and n, respectively. The spin wave stiffness is represented by D_{sw}, and $\hbar$ corresponds to the reduced Planck constant. Using this relation, with $n = 1$, $M_s = 1240$ kA m^{-1}, $K_s = 0.70$ mJ m^{-2}, and $B_{app} = 72$ mT, the data in Fig. 4(b) can be fitted, using the spin wave stiffness as the fitting parameter. Looking at the fitted curve (solid red curve), it can be seen that the measured data are not well described by the dispersion relation of Eq. (6). The measured dispersion is flattened out with respect to the theoretical behavior. This suggests, as was seen for the Kittel fits in Fig. 3(a), that there is an additional thickness dependence that is not captured by the dispersion relation in Eq. (6). A detailed investigation of this additional thickness dependence is out of the scope of this paper, however, a short discussion on a possible explanation will be given.

In the case of $n > 0$, the dispersion relation shown in Eq. (6) is dominated by the D_{sw} term. Therefore, an additional thickness dependence can be expected to be present in this spin wave stiffness. The spin wave stiffness itself is related to the exchange constant A_{ex} via the atomic spin S and the lattice constant a,

$$D_{sw} = \frac{A_{ex}a^3}{S}. \quad (8)$$

It has been demonstrated by Enrich *et al.* that the exchange constant in Co decreases when it is alloyed with other materials [25]. Moreover, they demonstrated a significant decrease of the average exchange constant of the Co layers in a Co/Ru multilayer for Co thicknesses below 10 nm. The decrease of A_{ex} was attributed to intermixed interface regions that have a lower exchange constant, which become more dominant for the thinner Co layers. In the case of the sputter-deposited structures measured here, interface intermixing is expected to occur as well. Since the data presented in Ref. [25] suggest an exponential dependence of A_{ex} on the Co thickness, the following estimation is used,

$$D_{sw}(t) = D_{sw,\infty}\left(1 - e^{-\frac{t}{d_0}}\right). \quad (9)$$

Substituting Eq. (9) into the dispersion relation, the measured spin wave frequencies are fitted with much more accuracy, as is shown by the dotted curve in Fig. 4(b). The fitted parameters are $D_{sw,\infty} = 980 \pm 30$ meV Å^2 and $d_0 = 4.7 \pm 0.3$ nm. The d_0 value seems to be reasonable compared to the data on A_{ex} in Ref. [25] (estimated value of $d_0 \approx 4.3$ nm). However, the value for $D_{sw,\infty}$, i.e., for bulk Co, is almost a factor of 3 higher than the expected value of 340 ± 75 meV Å^2 found for polycrystalline Co [26]. This discrepancy suggests that the

description of the spin wave stiffness as given in Eq. (9) is not complete and a more elaborate study is needed.

The thickness-dependent exchange constant being the cause of the observed (flattened) THz dispersion is an assumption that needs to be confirmed, however, it does also give a possible explanation for the discrepancies observed for the fundamental precessions shown in Fig. 3(a). The Curie temperature of a magnetic layer is directly proportional to the exchange constant, meaning that a lowering in the exchange constant results in a decrease of the Curie temperature. Since the measurements are performed at room temperature, this decreases the saturation magnetization and with it the precession frequency. As was mentioned earlier, adding such a thickness-dependent M_s to Eq. (1) indeed results in a better fit to the measured data (analysis in Supplemental Material Sec. III [22]). This shows that the additional thickness dependence observed in the dispersion of both the fundamental precessions as well as the spin waves can be explained with a thickness dependence in the average exchange constant of the Co film, possibly caused by intermixing in the interface regions.

B. Spin current generation

Next, the laser-pulse excited spin current generation in the OOP layer is investigated. This is done by measuring the efficiency and canting angle as a function of the OOP layer thickness. For this measurement, four structures are fabricated, following the basic noncollinear bilayer as introduced earlier. Each structure has a similar top Co layer with $t_{Co} = 3$ nm, but a different amount of $[Co/Ni]_N$ repeats. The used repeats are $N = 1$, 2, 3, and 4. Unfortunately, the measurements on the structure with $N = 1$ showed no precessions of the IP layer. Polar hysteresis measurements on this structure revealed a very small coercivity for the OOP layer ($\approx$1 mT), indicating weak PMA. As a result, the OOP layer is pulled in plane by the applied field during the measurements. In this case, parallel spins are injected in the IP layer and there will be no STT and thus no canting of the magnetization. This is seen in the measurements by the absence of both the demagnetization and the precession. Although this causes the structure to be useless for the spin current investigation, it confirms again that the measured precession of the IP magnetization is indeed caused by the STT mechanism.

The samples with $N = 2$, 3, and 4 did show sufficient PMA and the efficiency and canting angle could be determined. The resulting ϵ and $\theta_{c,\%}$ as functions of the $[Co/Ni]_N$ repeats are shown in Fig. 5 (dotted lines are guides to the eye). First, by looking at the efficiency, it can be seen that there seems to be no strong dependency on the thickness of the OOP layer. A constant efficiency would mean that for an equal amount of angular momentum lost in the OOP layer, an equal amount of angular momentum is absorbed by the IP layer, independent of the thickness of the OOP layer. This behavior can also be seen in the measured $\theta_{c,\%}$ as a function of $[Co/Ni]_N$ repeats, shown in the inset. The amount of angular moment lost in the OOP layer per percent demagnetization increases with the amount of repeats. With a constant ϵ, the amount of angular momentum absorbed in the IP layer will also increase with the $[Co/Ni]_N$ repeats, resulting in a rise of $\theta_{c,\%}$. Due to the limited number of thicknesses available here, a more elaborate study is needed to confirm the observed behavior of ϵ and $\theta_{c,\%}$. However, the presented observations do allow for speculations on the spin current generation mechanism.

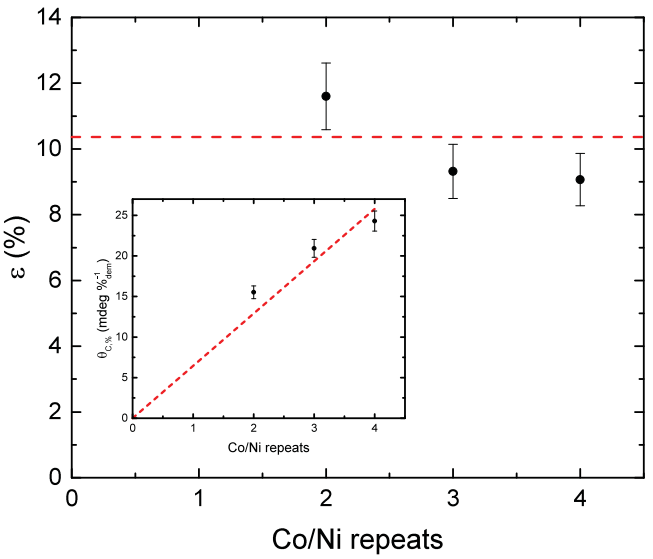

FIG. 5. Efficiency and canting angle per percent demagnetization (inset) measured on the noncollinear bilayers with $t_{Co} = 3$ nm and $[Co/Ni]_N$ repeats of $N = 2$,3 and 4. For the efficiency no significant dependence on the amount of repeats is seen, whereas for the canting angle per percent demagnetization a clear increase with number of repeats is present. The dotted lines are guides to the eye.

It is noted that the stacks (spacer layer and top Co layer) deposited on top of the different $[Co/Ni]_N$ repeats are designed to be identical. This means that the transport and absorption of the spin current generated in the OOP layer are expected to be the same in all three structures. The absence of a clear thickness dependence in ϵ therefore indicates that a similar amount of angular momentum loss in the OOP layer generates a similar spin current, independent of the thickness of the OOP layer. Also, it implies that the full thickness of the OOP layer contributes to the generated spin current. The latter notion contradicts the idea of a limited interface region ($\approx$1 nm) contributing to the spin current generation, as was suggested by Alekhin *et al.* for Fe/Au [13]. In the case of a superdiffusive spin current, the spin current is generated due to spin filtering of the hot electrons in the magnetic layer [5]. Although for a complete assessment explicit calculations need to be performed, it might be expected that the spin filtering becomes more pronounced with increasing layer thickness since part of the hot electrons will have to travel a longer distance within the FM layer. In that case, the net spin current leaving the OOP layer would increase with the layer thickness, resulting in an increase of the efficiency with $[Co/Ni]_N$ repeats. This, however, is not observed in the present measurement. The spin current generated by the spin-dependent Seebeck effect is negligible in the structures used in this paper, as was demonstrated by Schellekens *et al.* for similar noncollinear bilayers [14]. The notion of the generated spin current being solely dependent on the amount of lost angular momentum does agree with a mechanism where the spin current is

generated by the demagnetization, thus following dM/dt [15]. In this case, a certain amount of loss in angular momentum in the OOP layer (dM) will generate a certain (diffuse) spin current, independent of the thickness of the OOP layer. While this analysis tentatively points towards a dM/dt-like scenario, the main conclusion is that the type of experiments presented can be highly valuable to resolve the optical-STT mechanism. Explicit model calculations for the different scenarios need to be performed before making an unambiguous assignment.

IV. CONCLUSION

In conclusion, both the generation and absorption of fs laser-pulse induced spin currents have been experimentally investigated using noncollinear magnetic bilayers. Using a wedge-shaped Co (absorption) layer, it has been demonstrated that the spin current is absorbed very locally near the injection interface (90% within the first ≈2 nm). This local absorption was confirmed by the demonstration of THz spin waves being excited within the Co layer as a result of the strong gradient in the canting angle of the IP magnetization after the optical excitation. Also, the mechanism behind the optical spin current generation in these magnetic bilayers has been examined. This was done by measuring the spin current generation as a function of the Co/Ni (generation) layer thickness. The results indicate that the spin current generation is solely dependent on the amount of lost angular momentum, and not on the thickness of the layer, favoring a mechanism where the spin current is generated by the demagnetization, and follows dM/dt. The experiments presented in this paper demonstrate that the noncollinear bilayer is a convenient structure to investigate optically generated spin currents. Moreover, the possibility to excite THz spin waves in these structures causes them to be of high potential for future THz magnonics.

ACKNOWLEDGMENT

This work is part of the Gravitation program "Research Centre for Integrated Nanophotonics," which is financed by the Netherlands Organisation for Scientific Research (NWO).

[1] E. Beaurepaire, J.-C. Merle, A. Daunois, and J.-Y. Bigot, Ultrafast Spin Dynamics in Ferromagnetic Nickel, Phys. Rev. Lett. **76**, 4250 (1996).

[2] B. Koopmans, G. Malinowski, F. D. Longa, D. Steiauf, M. Fahnle, T. Roth, M. Cinchetti, and M. Aeschlimann, Explaining the paradoxical diversity of ultrafast laser-induced demagnetization, Nat. Mater. **9**, 259 (2010).

[3] B. Y. Mueller, A. Baral, S. Vollmar, M. Cinchetti, M. Aeschlimann, H. C. Schneider, and B. Rethfeld, Feedback Effect during Ultrafast Demagnetization Dynamics in Ferromagnets, Phys. Rev. Lett. **111**, 167204 (2013).

[4] K. Carva, M. Battiato, D. Legut, and P. M. Oppeneer, *Ab initio* theory of electron-phonon mediated ultrafast spin relaxation of laser-excited hot electrons in transition-metal ferromagnets, Phys. Rev. B **87**, 184425 (2013).

[5] M. Battiato, K. Carva, and P. M. Oppeneer, Superdiffusive Spin Transport as a Mechanism of Ultrafast Demagnetization, Phys. Rev. Lett. **105**, 027203 (2010).

[6] M. Battiato, K. Carva, and P. M. Oppeneer, Theory of laser-induced ultrafast superdiffusive spin transport in layered heterostructures, Phys. Rev. B **86**, 024404 (2012).

[7] C. D. Stanciu, F. Hansteen, A. V. Kimel, A. Kirilyuk, A. Tsukamoto, A. Itoh, and Th. Rasing, All-Optical Magnetic Recording with Circularly Polarized Light, Phys. Rev. Lett. **99**, 047601 (2007).

[8] S. Mangin, M. Gottwald, C.-H. Lambert, D. Steil, V. Uhlr, L. Pang, M. Hehn, S. Alebrand, M. Cinchetti, G. Malinowski, Y. Fainman, M. Aeschlimann, and E. E. Fullerton, Engineered materials for all-optical helicity-dependent magnetic switching, Nat. Mater. **13**, 286 (2014).

[9] C.-H. Lambert, S. Mangin, B. S. D. Ch. S. Varaprasad, Y. K. Takahashi, M. Hehn, M. Cinchetti, G. Malinowski, K. Hono, Y. Fainman, M. Aeschlimann, and E. E. Fullerton, All-optical control of ferromagnetic thin films and nanostructures, Science **345**, 1337 (2014).

[10] G. Malinowski, F. D. Longa, J. H. H. Rietjens, P. V. Paluskar, R. Huijink, H. J. M. Swagten, and B. Koopmans, Control of speed and efficiency of ultrafast demagnetization by direct transfer of spin angular momentum, Nat. Phys. **4**, 855 (2008).

[11] A. Melnikov, I. Razdolski, T. O. Wehling, E. Th. Papaioannou, V. Roddatis, P. Fumagalli, O. Aktsipetrov, A. I. Lichtenstein, and U. Bovensiepen, Ultrafast Transport of Laser-Excited Spin-Polarized Carriers in Au/Fe/MgO(001), Phys. Rev. Lett. **107**, 076601 (2011).

[12] D. Rudolf, C. La-O-Vorakiat, M. Battiato, R. Adam, J. M. Shaw, E. Turgut, P. Maldonado, S. Mathias, P. Grychtol, H. T. Nembach, T. J. Silva, M. Aeschlimann, H. C. Kapteyn, M. M. Murnane, C. M. Schneider, and P. M. Oppeneer, Ultrafast magnetization enhancement in metallic multilayers driven by superdiffusive spin current, Nat. Commun. **3**, 1037 (2012).

[13] A. Alekhin, D. Bürstel, A. Melnikov, D. Diesing, and U. Bovensiepen, *Ultrafast Laser-Excited Spin Transport in Au/Fe/MgO(001), Relevance of the Fe Layer Thickness, in Ultrafast Magnetism I*, edited by J.-Y. Bigot, W. Hübner, T. Rasing, and R. Chantrell, Springer Proceedings in Physics Vol. 159 (Springer, Berlin, 2015), p. 241.

[14] A. J. Schellekens, K. C. Kuiper, R. R. J. C. de Wit, and B. Koopmans, Ultrafast spin-transfer torque driven by femtosecond pulsed-laser excitation, Nat. Commun. **5**, 4333 (2014).

[15] G.-M. Choi, B.-C. Min, K.-J. Lee, and D. G. Cahill, Spin current generated by thermally driven ultrafast demagnetization, Nat. Commun. **5**, 4334 (2014).

[16] G.-M. Choi, C.-H. Moon, B.-C. Min, K.-J. Lee, and D. G. Cahill, Thermal spin-transfer torque driven by the spin-dependent Seebeck effect in metallic spin valves, Nat. Phys. **11**, 576 (2015).

[17] I. Razdolski, A. Alekhin, N. Ilin, J. P. Meyburg, V. Roddatis, D. Diesing, U. Bovensiepen, and A. Melnikov, Nanoscale interface confinement of ultrafast spin transfer torque driving non-uniform spin dynamics, Nat. Commun. **8**, 15007 (2017).

[18] M. Krawczyk and D. Grundler, Review and prospects of magnonic crystals and devices with reprogrammable band structure, J. Phys.: Condens. Matter **26**, 123202 (2014).

[19] A. V. Chumak, V. I. Vasyuchka, A. A. Serga, and B. Hillebrands, Magnon spintronics, Nat. Phys. **11**, 453 (2015).

[20] M. T. Johnson, P. J. H. Bloemen, F. J. A. den Broeder, and J. J. de Vries, Magnetic anisotropy in metallic multilayers, Rep. Prog. Phys. **59**, 1409 (1996).

[21] M. van Kampen, C. Jozsa, J. T. Kohlhepp, P. LeClair, L. Lagae, W. J. M. de Jonge, and B. Koopmans, All-Optical Probe of Coherent Spin Waves, Phys. Rev. Lett. **88**, 227201 (2002).

[22] See Supplemental Material at http://link.aps.org/supplemental/10.1103/PhysRevB.96.014417 for a discussion on how the efficiency and canting angle are calculated from a typical precession measurement, a derivation of the spin wave dispersion relation, and an additional analysis of the transverse spin current absorption, including a thickness-dependent saturation magnetization.

[23] T. Taniguchi, S. Yakata, H. Imamura, and Y. Ando, Penetration depth of transverse spin current in ferromagnetic metals, IEEE Trans. Magn. **44**, 2636 (2008).

[24] A. J. Schellekens, N. de Vries, J. Lucassen, and B. Koopmans, Exploring laser-induced interlayer spin transfer by an all-optical method, Phys. Rev. B **90**, 104429 (2014).

[25] C. Eyrich, A. Zamani, W. Huttema, M. Arora, D. Harrison, F. Rashidi, D. Broun, B. Heinrich, O. Mryasov, M. Ahlberg, O. Karis, P. E. Jönsson, M. From, X. Zhu, and E. Girt, Effects of substitution on the exchange stiffness and magnetization of Co films, Phys. Rev. B **90**, 235408 (2014).

[26] S. P. Vernon, S. M. Lindsay, and M. B. Stearns, Brillouin scattering from thermal magnons in a thin Co film, Phys. Rev. B **29**, 4439 (1984).